Acta Oceanol. Sin., 2021, Vol. 40, No. 3, P. 1–17
https://doi.org/10.1007/s13131-021-1720-7
http://www.hyxb.org.cn
E-mail: hyxbe@263.net

Spatiotemporal characteristics of sea ice transport in the Baffin Bay and its association with atmospheric variability

Weifu Sun[1], Haibo Bi[2, 3*], Min Fu[4], Xi Liang[4], Yunhe Wang[3*], Yu Liang[3, 5], Jue Huang[7], Haijun Huang[3, 5], Liwen Yan[3, 5], Qinglong Yu[4], Shuang Liang[6]

[1] Oceanic Telemetry Engineering and Technology Innovation Center, First Institute of Oceanography, Ministry of Natural Resources, Qingdao 266061, China

[2] Laboratory for Marine Geology, Pilot National Laboratory for Marine Science and Technology (Qingdao), Qingdao 266037, China

[3] Center for Ocean Mega-Science & Key Laboratory of Marine Geology and Environment, Institute of Oceanology, Chinese Academy of Sciences, Qingdao 266071, China

[4] National Marine Environmental Forecasting Center, Beijing 100081, China

[5] University of Chinese Academy of Sciences, Beijing 100049, China

[6] Aerospace Information Research Institute, Chinese Academy of Sciences, Beijing 100094, China

[7] College of Geodesy and Geomatics, Shandong University of Sicence and Technology, Qingdao 266590, China

Received 3 May 2020; accepted 6 July 2020

Abstract

Sea ice export through the Baffin Bay plays a vital role in modulating the sea ice cover variability in the Labrador Sea. In this study, satellite-derived sea ice products are used to obtain the sea ice area flux (SIAF) through the three passages in the Baffin Bay (referred to as A, B, and C for the north, middle, and south passages, respectively). The spatial variability of the monthly sea ice drift in the Baffin Bay is presented. The interannual variability and trends in SIAF via the three passages are outlined. The connection to several large-scale atmospheric circulation modes is assessed. Over the period of 1988–2015, the average annual (October to the following September) SIAF amounts to 555×10^3 km^2, 642×10^3 km^2, and 551×10^3 km^2 through Passages A, B, and C, respectively. These quantities are less than that observed through the Fram Strait (FS, 707×10^3 km^2) of the corresponding period. The positive trends in annual SIAF, on the order of 53.1×10^3 km^2/(10 a) and 43.2×10^3 km^2/(10 a) (significant at the 95% confidence level), are identified at Passages A and B, respectively. The trend of the south passage (C), however, is slightly negative (-13.3×10^3 km^2/(10 a), not statistically significant). The positive trends in annual SIAF through the Passages A and B are primarily attributable to the significant increases after 2000. The connection between the Baffin Bay sea ice export and the North Atlantic Oscillation is not significant over the studied period. By contrast, the association with the cross-gate sea level pressure difference is robust in the Baffin Bay (R equals 0.69 to 0.71, depending on the passages considered), but relatively weaker than that over FS (R=0.74).

Key words: sea ice transport, Baffin Bay, Arctic, sea ice area flux (SIAF)

Citation: Sun Weifu, Bi Haibo, Fu Min, Liang Xi, Wang Yunhe, Liang Yu, Huang Jue, Huang Haijun, Yan Liwen, Yu Qinglong, Liang Shuang. 2021. Spatiotemporal characteristics of sea ice transport in the Baffin Bay and its association with atmospheric variability. Acta Oceanologica Sinica, 40(3): 1–17, doi: 10.1007/s13131-021-1720-7

1 Introduction

The Baffin Bay is a semi-enclosed ocean basin between Baffin Island and Greenland that connects the Arctic Ocean and the Northwest Atlantic Ocean. Sea ice outflow through the Davis Strait is a key component of the freshwater budget insert a space into the Labrador Sea. The anomalous outflows of sea ice could contribute to the freshening of upper waters of the Labrador Current (Goosse et al., 1997; Curry et al., 2014; Yang et al., 2016). In addition, sea ice export via the Davis Strait modulates the sea ice cover variations in the Labrador Sea and thereby influences the summer atmospheric variability over a larger domain (Wu et al., 2013). Moreover, the physical properties of productive coast banks and slope areas (Hansen et al., 2003; Drinkwater, 2009) can be altered by the sea ice export of Baffin Bay, and thus the North Atlantic ecosystem could be affected.

A robust trend of the warmer atmosphere been observed in the Pan-Arctic area since the late 1990s (Serreze et al., 2009; Stroeve et al., 2014, 2018; Graham et al., 2017), involving the Baffin

Foundation item: The National Key Research and Development Program of China under contract Nos 2016YFA0600102, 2017YFC1405106, 2016YFC1402707, and 2019YFE0114800; the General Project of Natural Science Foundation of Shandong Province under contract No. ZR2020MD100; the Key Deployment Project of Centre for Ocean Mega Science, Chinese Academy of Sciences, under contract No. COMS2020Q12; the National Natural Science Foundation of China under contract Nos 42076185 and 41406215; the Open Fund for the Key Laboratory of Marine Geology and Environment, Institute of Oceanology, Chinese Academy of Sciences under contract No. MGE2020KG04; the Key R&D Project of Shandong Province under contract No. 2019GSF111017; the NSFC-Shandong Joint Fund for Marine Science Research Centers under contract No. U1606401.
*Corresponding author, E-mail: bhb@qdio.ac.cn; wangyunhe@qdio.ac.cn

Bay with a rate of 2–3°C/(10 a) (Peterson and Pettipas, 2013). Prolonged days of sea ice melting, as indicated by the earlier melting onset and delayed ice-freezing startup dates, are identified in the Baffin Bay (Stroeve et al., 2014). Coincidently, a rapid shrinkage of sea ice cover in all seasons is also found over the bay (Comiso et al., 2017b; Parkinson and Cavalieri, 2002). Within the context of rapid climate changes, the examination of the spatiotemporal characteristics of the sea ice export via the Baffin Bay is of particular interests.

Compared with the sparsely distributed *in-situ* measurements, satellite observations are unique owing to the capability to capture the daily changes of polar sea ice cover (Comiso and Hall, 2014; Parkinson, 2014; Tilling et al., 2016; Parkinson and Cavalieri, 2002). Sea ice area flux (SIAF) has been investigated in several key water passages located on the periphery of the Arctic Basin, such as the Fram Strait (FS), Laptev Sea, Nares Strait. (Kwok et al., 2005, 2010, 2013; Spreen et al., 2006; Kwok, 2007, 2009; Smedsrud et al., 2011, 2017; Krumpen et al., 2013, 2016; Bi et al., 2016a, b; Zhang et al., 2017). Among them, FS serves as a primary passage of sea ice export and is associated with the overall variations in the Arctic sea ice coverage (Smedsrud et al., 2011, 2017). Sea ice transport via the Davis Strait (southern fluxgate of the Baffin Bay) was previously examined, but was only limted to a short period owing to the lacking of observations (Cuny et al., 2005; Kwok, 2007; Curry et al., 2014). Recently, the SIAF trends of a long-term via the Baffin Bay over the past several decades were examined by Bi et al. (2019). In that study, the increase in sea ice outflow via the bay were reported to be attributable to the increase in the drag coefficient of sea ice surface together with the decline in sea ice thickness.

Complementary to the study conducted by Bi et al. (2019), which primarily focused on the trends in SIAF, in this study we attempt to outline the spatiotemporal characteristics with regard to the sea ice export across the Baffin Bay. The SIAF is analyzed in terms of their seasonal and annual variability. Moreover, the decadal SIAF changes between the two periods (1988–2000 and 2001–2015) are examined. The two periods are considered because of the occurrence of a radical shift in the Arctic climate since the turn of the new century (Zhang et al., 2008). Besides, the connection of the Baffin Bay SIAF with the typical large-scale atmospheric circulation mode, as represented by North Atlantic Oscillation (NAO), is assessed, which is also not mentioned in the study of Bi et al. (2019).

This study is organized as follows. Section 2 describes the data and methodology used to calculate the SIAF and provides the corresponding uncertainty estimate. Section 3 presents the variability and trends in the accumulated SIAF fields at the three passages, and a comparison with the estimates via the FS is depicted in this section. Section 4 outlines the associations of the SIAF through the Baffin Bay with some typical climate elements (surface winds (SW), sea level pressure (SLP), surface air temperature (SAT), and sea surface temperature (SST)). Moreover, the linkage with local and large-scale atmospheric variability, including the North Atlantic Oscillation (NAO) and cross-gate sea level pressure difference (SLPD), is discussed in this section. Section 5 concludes this study.

2 Data and methods

2.1 *Data*

2.1.1 *Sea ice motion*

One of the most comprehensive sea ice motion (SIM) datasets is provided by the National Snow and Ice Data Center (NSIDC) (Tschudi et al., 2019). This product has contributed to many studies associated with polar sea ice changes and has been widely adopted by the modeling and data assimilation communities (http://nsidc.org/data/NSIDC-0116). This dataset is derived from a variety of satellite-based sensors, including the Advanced Very High Resolution Radiometer (AVHRR), the Scanning Multichannel Microwave Radiometer (SMMR), Special Sensor Microwave Imager (SSM/I), the Special Sensor Microwave Imager Sounder (SSMIS), and the Advanced Microwave Scanning Radiometer-Earth Observing System (AMSR-E), merged with buoy measurements from the International Arctic Buoy Program (IABP) and estimates determined from the reanalyzed wind data.

The daily 25 km EASE-Grid SIM vectors over the period from 1978 to 2015 is provided by NSIDC (Tschudi et al., 2019). The SIM is retrieved using the maximum correlation coefficient (MCC) method. That is, MCC measures the correlation of the pixel groups between image pairs. The correlation is calculated between the target area with $N \times N$ pixels in one image and the areas of the same size within the sourrounding region in the consecutive image. The displacement of the ice is then defined by the location where the correlation coefficient is the highest.

Note that the satellite sensor on the SMMR was operated only on alternate days due to spacecraft power limitations. Thus, these earlier observations were only collected every other day for the period from October 1978 to August 1987. In this case, half of the daily satellite-derived SIM, as well as sea ice concentration (SIC) records, dismissed and hampers the ability to obtain an accurate estimate for the monthly SIAF before 1987. After the launch and operation of the SSM/I since July 1987, daily satellite observations of sea ice became available. Also, previous studies reported that the lower SIAF estimate in FS area based on the SIM data from NSDIC seems to be unrealistic over the period before 1987 (Bi et al., 2016b; Smedsrud et al., 2017). A noticeable discontinuity is found between the NSDIC sea ice motion record based on observations from the SMMR and subsequent SSM/I series. To reduce the uncertainty caused by the shifting of satellite sensors, we use only the NSIDC daily SIM data during the period of 1988–2015.

2.1.2 *Sea ice concentration*

SIC data were also obtained from the NSIDC (http://nsidc.org/data/NSIDC-0079). These data are derived from the SMMR onboard the Nimbus-7 satellite, the SSM/I onboard the Defense Meteorological Satellite Program (DMSP)-F8, -F11, -F13, and SSMIS aboard DMSP-F17 by applying the Bootstrap algorithm (Comiso et al., 2017a). This dataset provides an improved consistency between sensors through the use of a suite of daily varying tie points generated from the AMSR-E observations. Also, the product provides an enhanced removal of weather and land contamination. A climatological SST mask was applied to remove spurious sea ice pixels from regions where the ocean surface is above freezing. Additionally, land contamination (false ice along the coast due to pixels containing a mixture of land and ocean) were removed using a filter adapted from Cho et al. (1996). Daily SIC data (1988–2015) used in this study were available on a 25 km polar stereographic grid.

2.1.3 *SLPD and NAO*

The SLP product is obtained from the National Centers for Environmental Prediction/National Center for Atmospheric Re-

search (NCEP/NCAR) (https://www.esrl.noaa.gov/psd/cgi-bin/db_search/DBListFiles.pl?did=195&tid=61156&vid=675) reanalysis data (Kalnay et al., 1996). SLPD is calculated as the SLP difference between the western and eastern endpoints of a passage (lines as marked in Fig. 1, Passage A: (73.6°N, 77.1°W) to (75.9°N, 68.0°W); B: (70.2°N, 67.4°W) to (71.4°N, 55.9°W); C: (66.7°N, 61.1°W) to (67.2°N, 54.1°W)). The atmospheric structure linked to positive/negative SLPD phases (SLPD+/–) indicates ice export/import through a passage.

The NAO index is acquired from the NCEP Climate Prediction Center (CPC) (http://www.cpc.ncep.noaa.gov/products/precip/CWlink/pna/nao_index.html). It represents a climatic phenomenon in the North Atlantic Ocean associated with fluctuations between the Icelandic low and the Azores high (Hurrell, 1995). It captures the primary variations (approximately 30%) of the monthly SLP all year round in the North Atlantic regions. Ideally, an intense Icelandic low with a strong Azores ridge to its south leads to a positive NAO mode (i.e., NAO+), which could enhance the sea ice extent in the Baffin Bay (Stern and Heide-Jørgensen, 2003). By contrast, a positive SLP anomaly over the Icelandic low during the negative phase (NAO–) would reduce the ice extent through the bay (Stern and Heide-Jørgensen, 2003). However, the connection between the NAO and sea ice transport over the Baffin Bay region remains unclear (Häkkinen and Cavalieri, 2005).

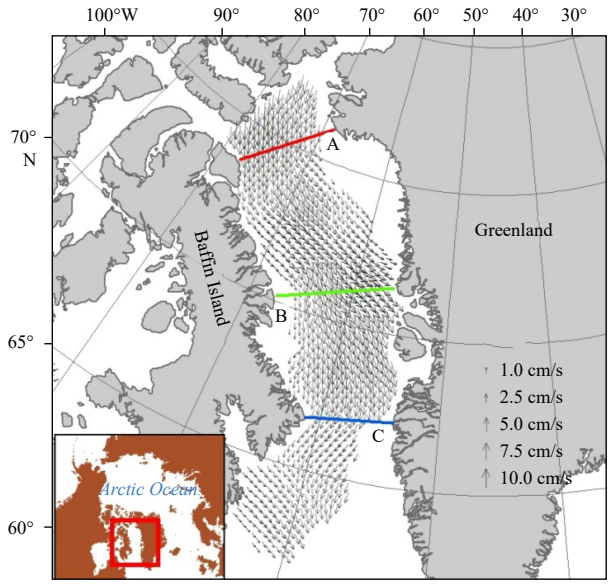

Fig. 1. Locations of passages used to obtain the SIAF over the Baffin Bay. Passages A (red line), B (green line), and C (blue line) are positioned in the northern, middle, and southern sides, respectively. The inset map points to the general location of our study area from a broader view. The black arrows denote the SIM vectors. This is an example of the monthly-mean daily sea ice drift fields (March 1, 2015).

2.2 *SIAF calculation and uncertainty assessment*

SIAF is estimated as the integral of the product between the gate-perpendicular components of the SIM and SIC along a gate (Kwok, 2007). To inspect the contrast of the SIAF variability, three passages are considered (A, B, and C, as shown in Fig. 1), located at the northern, middle, and southern Baffin Bay, respectively. The north gate (A), which is about 372 km wide (red line in Fig. 1), is positioned aroud 73°N. The middle gate (B) is about 450 km wide and positioned around 67°N (green line in Fig. 1). The south gate (C) is about 440 km wide (blue line in Fig. 1) and located aroud 70°N.

The SIAF across one gate is calculated as follows:

$$\mathrm{SIAF} = G\sum_{i=1}^{N-1} u_i c_i (i = 1, 2, \cdots, N), \tag{1}$$

where N is the number of grids along the gate, and G corresponds to the grid size (25 km), u_i and c_i are SIM and SIC at the i-th grid along the gate. Passage A spans fourteen 25-km grids, while B and C cover eighteen and seventeen grids with a 25-km size, respectively. SIM at the endpoints of each passage, within a narrow zone of approximately 10 km, are constrained to zero (Kwok et al., 2004; Kwok, 2009).

The monthly SIAF refers to the cumulative results of the daily flux over a calendar month. Likewise, the annual SIAF denotes the cumulative monthly area flux of one year. With the assumption that uncertainty in the SIM grid samples is additive, unbiased, uncorrelated, and normally distributed (Kwok, 2009), the errors in the gate-integrated daily area flux estimate can be calculated as follows (Kwok, 2009): $\sigma_\mathrm{D} = \sigma_\mathrm{u} L/\sqrt{N_\mathrm{s}}$, where L is the width of a passage, σ_u is the uncertainty in daily SIM and N_s is the number of independent samples across a gate (Table 1). For σ_u, we use the upper limit of the uncertainty determined through comparisons with buoy drifts, and it corresponds to 1.73 km/d (or 2 cm/s) for the SIM data from NSIDC (Sumata et al., 2014). The uncertainty in the monthly area flux estimate is obtained with $\sigma_\mathrm{m} = \sigma_\mathrm{D}\sqrt{N_\mathrm{D}}$, where N_D is the number of days over the month considered. Thereby, the annual flux uncertainty is calculated as $\sigma_\mathrm{a} = \sigma_\mathrm{m}\sqrt{N_\mathrm{m}}$, where N_m=12 is the number of calendar months of a complete sea ice cycle of production and decay, from October to the following September. The annual export uncertainties σ_a correspond to 8.23%, 9.32%, 11.66% of the mean annual SIAFs over the period of 1988–2015 at the Passages A, B, and C, respectively (Table 1).

3 Results

3.1 *Comparisons to previous results*

Using SSM/I observations, Cuny et al. (2005) obtained the winter (December–May) SIAF through the Davis Strait over the period of 1991/1992–1999/2000. The results are presented in Fig. 2 (green line). For this decade, the mean winter (November–May) SIAF was estimated to 496×10³ km². In comparison, the average

Table 1. Uncertainty estimates of daily (σ_D), monthly (σ_m) and annually accumulated SIAF (σ_a) for the three passages over the period of 1988–2015

Passage	Width/km	N_s	σ_D/(10³ km²)	σ_m/(10³ km²)	σ_a/(10³ km²)
A	372	14	2.41	13.19	45.69
B	453	18	3.32	18.21	63.09
C	442	17	3.15	17.27	59.82

Note: N_s is the total numbers of grid covered by a passage.

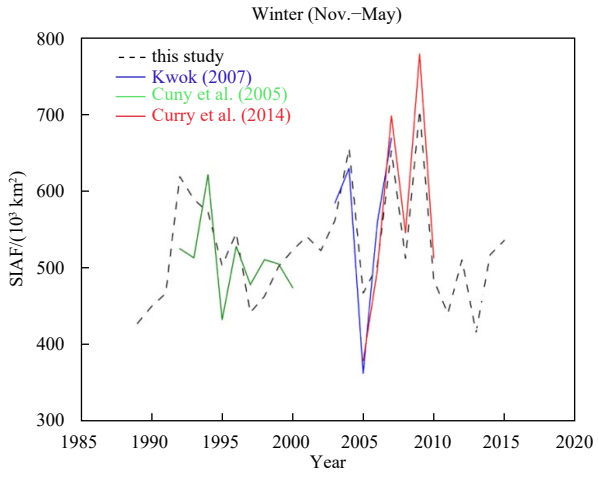

Fig. 2. Comparison between NSIDC-based SIAF estimates and those from preceding studies (Cuny et al., 2005; Kwok, 2007; Curry et al., 2014).

winter SIAF results of our study at Passage C (close to the Davis Strait) for the same period is 486×10³ km², slightly lower by (–10±50.4) km² compared to that of Cuny et al. (2005). The number after ± denotes the standard deviation of the difference. A moderate correlation (R=0.56) is found between the two records, which is associated with the contrast in the spatial resolution of the SIM data utilized. The product derived from SSM/I 37 GHz has a grid size of ~70 km while the size of the NSIDC data is characterized with 25 km.

Kwok (2007) adopted the AMSR-E 89 GHz data to retrieve SIM fields and calculated the sea ice export throuth the Baffin Bay over the period of 2002/2003–2006/2007. Furthermore, Curry et al. (2014) extened the record to 2004/2005–2009/2010. Correlation anaysis indicates that SIM derived from AMSR-E observations can account for approximately 90% of the variance of the Envisat-derived high-resolution SIM results. In this study, a strong correlation is also identified between the winter (October–May) SIAF estimates derived from the NSIDC product and AMAR-E observations. As shown in Fig. 2, the correlation reaches to 0.87 (0.93) between our estimates and those provided by Kwok (2007) (Curry et al. (2014)). The NSIDC-based estimates for the averaged winter SIAF at Passage C (near the Davis Strait) is smaller by (–24.3±63.7) ×10³ km² than that provided by Kwok (2007), and less by (–45.5±61.0) ×10³ km² compared with estiamtes by Curry et al. (2014). However, these differences correspond to only a few percentages (about 4.5% and 8.9%) relative to the mean SIAF estimates based on the NSIDC sea ice products (approximately 511×10³ km²). Overall, a reasonably good agreement is noted between the NSIDC-based SIAF estimates and the previous results (Fig. 2).

3.2 *Spatial variability for ice drift*

3.2.1 *Sea ice drift pattern in the Baffin Bay*

The spatial pattern of the mean daily sea ice drift in the Baffin Bay for each month over the period of 1988–2015 is presented. As shown in Fig. 3, the prevailing sea ice drift pattern is southward and primarily confined to the west side of the bay. Larger SIM fields are observed during the winter months (October to May, with a basin-side mean of about 10 km/d) while smaller SIMs are identified during summer months (June to August, on average, about 1 km/d). From October to December, the sea ice coverage within the bay expands very quickly, and the SIM accelerates rapidly due to the stronger wind forcing (Figs 3j–l). During the late winter and early spring periods (January to April), the sea ice speeds approach to the peak (Figs 3a–d), especially over the regime in the southern Davis Strait, where the sea ice drift attains a rate of up to 15–20 km/d.

From the east towards the west side of the bay, an increase in the SIM fields is apparent. The SIM vectors along the west coast of Greenland are comparatively small and even reversed to northward in latitudes north of 70°N, forming an overall pattern of cyclonic sea ice transport in the northern Baffin Bay. This sort of distribution is linked to the cyclonic modes associated with the atmospheric circulaiton and oceanic currents in the bay (Melling et al., 2001). The southward sea ice transport is prominent during the winter months (October–May, Figs 3j–l and 3a–e). Although small in drift magnitude over the summer months (June–August, Figs 3f–h), the cyclonic sea ice transport pattern is also observable in the northern Baffin Bay.

3.2.2 *Cross-gate SIAF distribution*

The average southward components of the SIAF for each day over the period of 1988–2015 at different passages in the Baffin Bay are given in Fig. 4. For comparison, the SIAF fields for FS, around 79°N as used in Kwok (2007), are also presented. The coastal grids have been constrained to zero. The large standard deviation for each plot suggests the pronounced variability in the daily SIAF across the passages over the investigated period (Fig. 4).

In the north passage (Fig. 4a), the peak SIAF value of approximately 120 km²/d is located at a distance of 150 km from west, and gradually decreases to 92 km²/d at the distance of 330 km. Similar variations are also observed in the south passage (Fig. 4c), although with elongated SIAF distributions along the passage. This larger (smaller) ice speed in the west (east) half of the gate is associated with the cyclonic drift pattern in the northern Baffin Bay as mentioned above.

The cross-gate distribution of sea ice export in the middle passage (Fig. 4b) is symmetric, with the maximum daily SIAF observed around the central part (~105 km²/d). In the FS area, the SIAF distribution plot shows an increase from the west to the central grids (~150 km/d) and then a clear decrease is observed towards the east to 0 km/d (Fig. 4d).

3.3 *Variability and trend of accumulated SIAF through different passages*

3.3.1 *Daily SIAF variations*

The variability of the daily accumulated SIAF for each passage over the period of 1988–2015 is shown in Fig. 5 (thin black line). A 30-day smoothed SIAF is added in the plot. Generally, near-zero daily sea ice export occurs in warm seasons (June–September) while substantially enhanced daily SIAF (~3.0×10³ km²) occurs over the cold months (October to May). Moreover, significant decadal changes in Passages A and B are illustrated in Fig. 5 between the periods of 1988–2000 (red) and 2001–2015 (blue).

In the Baffin Bay, the temporal evolution of the daily SIAF fields for the three passages of the Baffin Bay is largely similar, but with differences in the details. Commonly, starting from zero outflow a clear autumn increase (October–December) is observed. It is followed by a relatively stable and large winter export during winter and early spring (January–April), and then by a rapid decrease in following spring and summer months toward the zero flux. Compared with the north, the south passage exhibits a smaller slope in the SIAF fields during the autumn months. Indeed, the autumn increase rates are 0.05×10³ km²/d, 0.04×10³ km²/d,

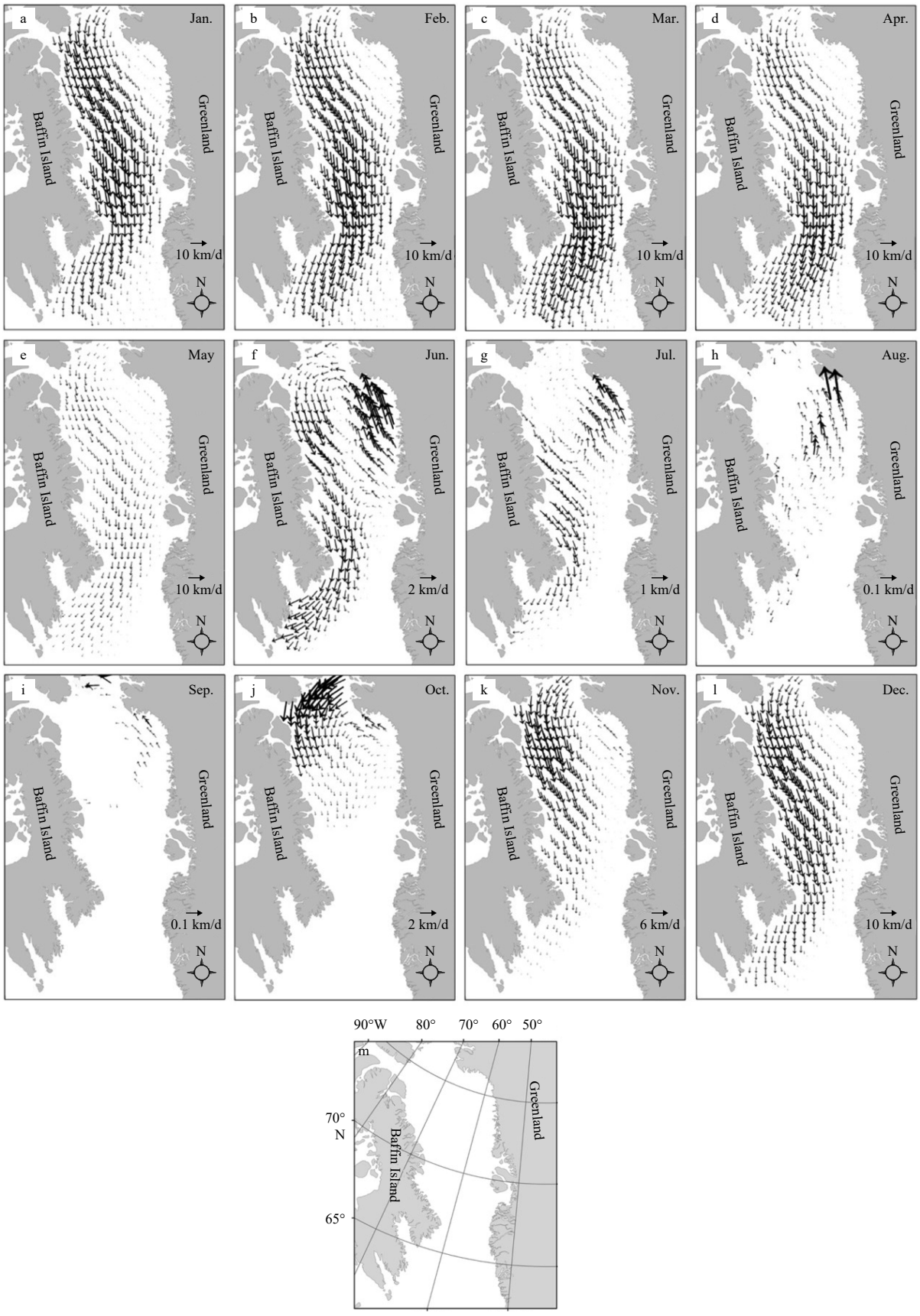

Fig. 3. Monthly-mean daily sea ice motion fields over the period of 1988–2015 in the Baffin Bay area (a–l), and the longtitue and latitude ranges of the studied region (m).

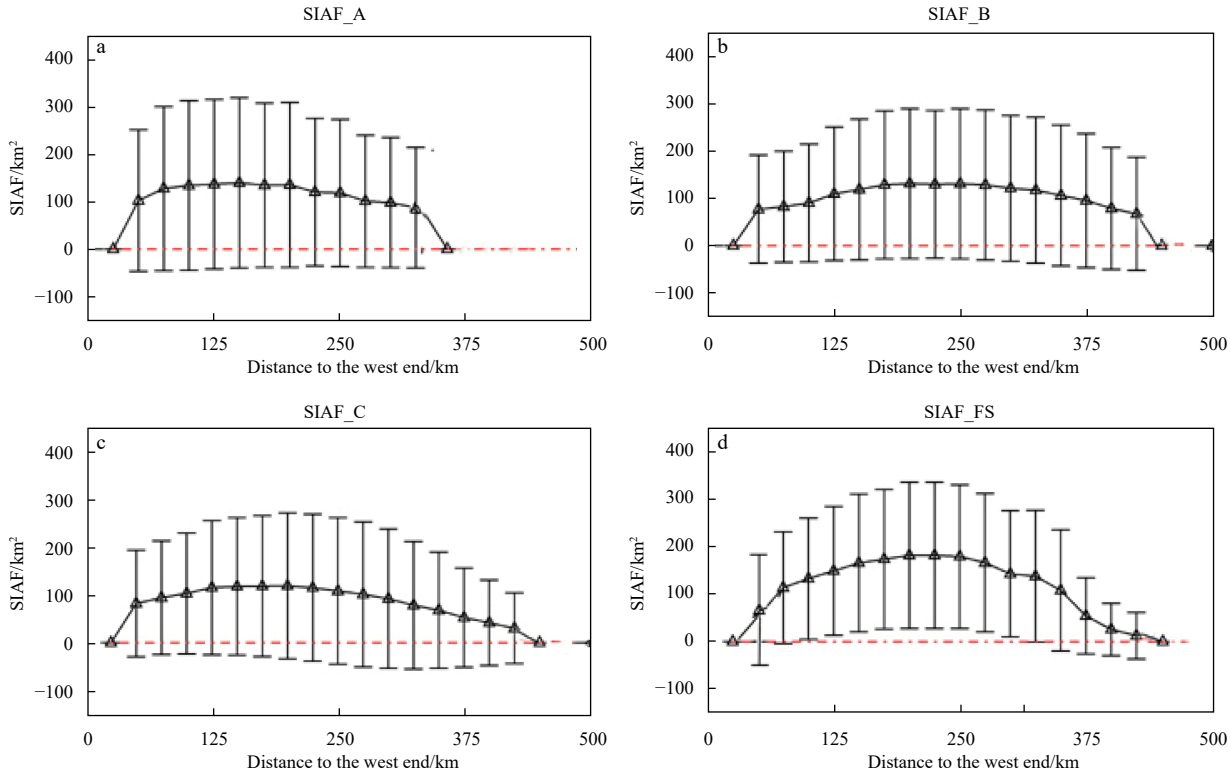

Fig. 4. Cross-gate distribution of the mean SIAF for each day over the period of 1988–2015. The standard deviation bars correspond to the variability of the daily SIAF estimates for the studied period. SIAF_A, SIAF_B, SIAF_C, and SIAF_FS denote the SIAF via the different Baffin Bay passages (A, B, and C) and Fram Strait, respectively.

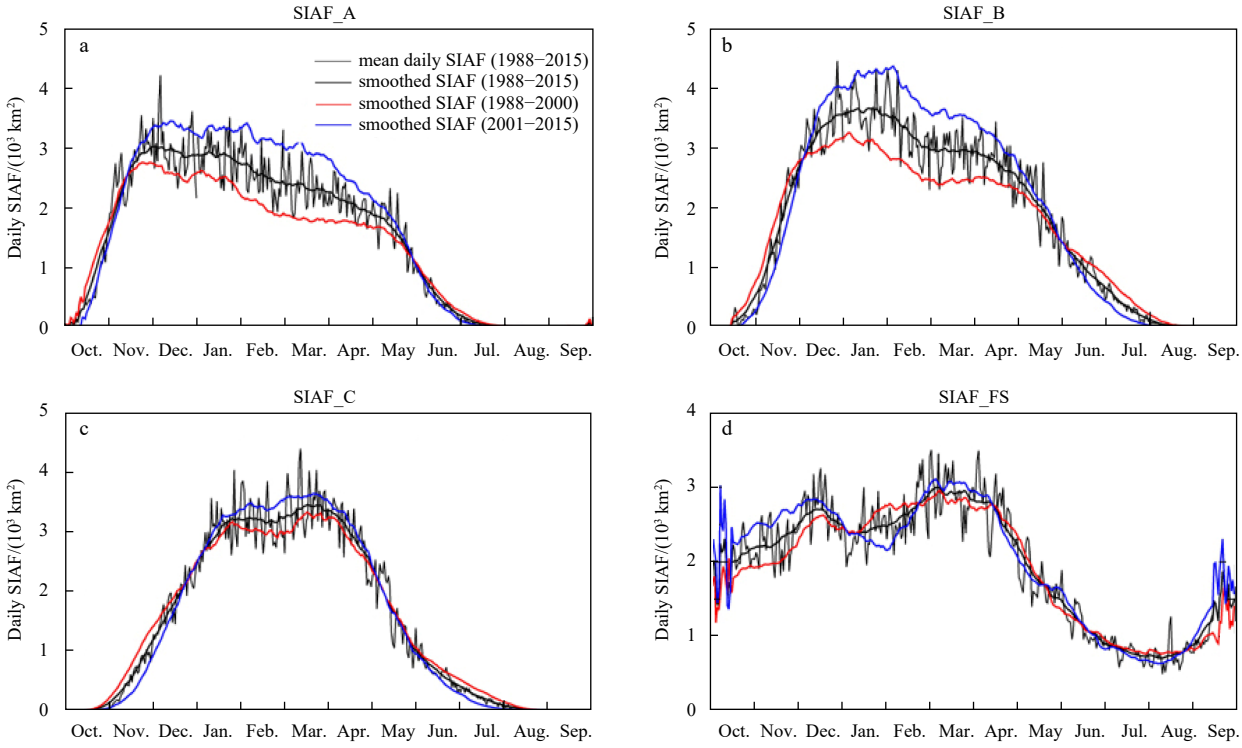

Fig. 5. Daily SIAF for different passages averaged over the period of 1988–2015. The SIAF through Passages A, B, and C in the Baffin Bay, and the FS are indicated in Figs 5a–d. The thin black line denotes the average daily SIAF through each passage, and the thick black line corresponds to the 30-day smoothed fields. The red and blue lines denote the 30-day smoothed SIAF fields for the periods before and after 2000, respectively.

and 0.03×10^3 km^2/d for the Passages A (Fig. 5a), B (Fig. 5b), and C (Fig. 5c), respectively. By contrast, the springtime decreasing slope of the daily SIAF fields is comparably small, with declining rates of -0.021×10^3 km^2/d, -0.023×10^3 km^2/d, and -0.024×10^3 km^2/d for Passages A, B, and C, respectively.

From late November until May, relatively large daily SIAFs, together with a slight decrease, are observed at the north passage (Fig. 5a) from ~3.0×10^3 km^2 to ~2.0×10^3 km^2, which corresponds to a rate of -0.005×10^3 km^2/d. This trend resembles the declining rate of the daily SIAF series (-0.048×10^3 km^2/d for December to April) in the middle passage (Fig. 5b), which also shows a double-peaks pattern (one in January and the other in April). In the south passage (Fig. 5c), relatively stable and high daily average ice export (3.20×10^3 km^2) appears during the months from mid-January to early April. Additionally, two peaks seem to exist in the south gates (one in late January and the other in late March). The shape of the daily SIAF time series for the middle passage (Fig. 5b) manifests itself as a transitional pattern between those of the north (Fig. 5a) and south passages (Fig. 5c). The SIAF variability in the FS shows a distinct pattern compared with the pattern in the Baffin Bay, particularly with the nonzero daily SIAF values (~0.5×10^3 km^2) during the summer months (Fig. 5d). The high sea ice export through the FS (on average, 2.6×10^3 km^2/d) is maintained for the cold months from October until May. Besides, two noticeable peaks, 2.6×10^3 km^2 (mid-December) and 2.8×10^3 km^2 (mid-March), are reflected in the daily SIAF fields of the FS (Fig. 5d).

As indicated in Figs 5a and b, decadal changes in the daily SIAF fields are prominent during the cold months in the north and middle passages. Compared with the earlier period (1988–2000), the recent (2001–2015) daily SIAF values in Passages A and B (Figs 5a and b, red and blue lines) increased by approximately 1.0×10^3 km^2 over the time period from December to April. In contrast, the decadal change in the south passages (Fig. 5c) is not readily identifiable. During the warm months, such as in the summer (June–July) and autumn (October–November) seasons, the daily SIAFs show reductions during the recent period by -0.20×10^3 km^2, -0.28×10^3 km^2, and -0.23×10^3 km^2 for the Passages A, B, and C, respectively. In the FS area, complex decadal changes occur in the daily SIAF fields (Fig. 5d). Apparently, a short-period increase of 0.5×10^3 km^2 from October to early December is found.

3.3.2 *Variability and trends in monthly accumulated sea ice export*

The monthly accumulated SIAFs through different passages of the Baffin Bay and the FS are shown in Fig. 6. For the winter months (October to May), the monthly SIAF is generally large at the three passages in the Baffin Bay. The maximum monthly SIAF fields for Passage A emerge in December (90×10^3 km^2), whereas the peak values for B and C occur later in January (110×10^3 km^2) and March (108×10^3 km^2), respectively. For the summer months (June to September), the SIAFs through the Baffin Bay passages are mostly negligible. The SIAF through the FS exhibits a steadily large value for the winter months (October to May, roughly 80×10^3 km^2/month), and notable ice exports during the summer months (June–September, ~30×10^3 km^2/month). The large standard deviations, as suggested in Fig. 6, confirm the significant interannual variations in the monthly SIAFs for each passage.

To further investigate the variability in the monthly SIAF at different passages, standardized SIAF fields (i.e., anomaly map) were calculated and are presented in Fig. 7. For Passages A and B,

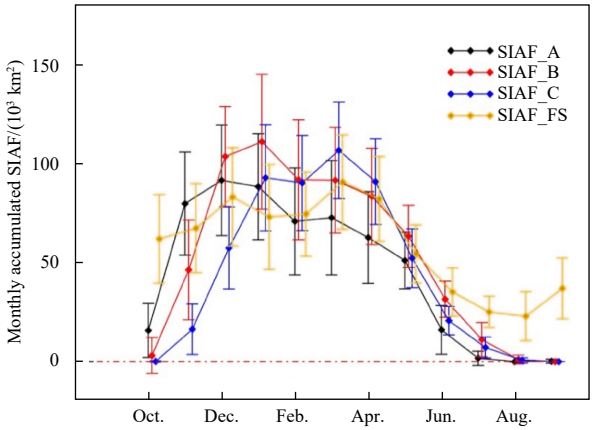

Fig. 6. Monthly accumulated SIAF for different passages averaged over the period of 1988–2015. Error bars correspond to the standard deviations of the monthly accumulated SIAF for the studied period.

the anomaly maps are broadly consistent (Fig. 7a vs. Fig. 7b). In particular, anomalous large sea ice exports principally occur during the winter months (October–May) over the period of 2003–2011 (Figs 7a and b). This is inconsistent with the lower-than-average monthly SIAF during the winter months before this period (1988–2002). Meanwhile, the three passages in the Baffin Bay experience a distinct decline in monthly SIAF during the summer months, as the ice started to vanish earlier and form later since the turn of the century owing to an increasingly warming climate. Passage C (Fig. 7c) and the FS (Fig. 7d) does not reveal a distribution pattern with anomaly fields that would favor any significant trend in wintertime monthly SIAF. The detailed statistical results are summarized in Table 2.

The monthly SIAF trends through the passage A presents opposite behavior for different seasons (Table 2). An increased SIAF trend predominates over most winter months (Table 2). However, during the summer months (June–August) the monthly SIAF fields basically display a declining trend, although any significance level is not reached (except July). Over this passage, all months show a significant decline in SIC, which is especially remarkable during the summer months (Table 2). The reduction in SIC may indicate a trend towards a looser ice pack, while reduced SIC also can promote a positive SIM trend (Eq. (1)). In general, the positive SIM trends over the winter months are generally accompanied by the negative SIC trends (Table 2 and Fig. 8). As a result, the positive SIM trends in winter largely cancel out the negative trends related to the reduced SIC, resulting in an overall increasing SIAF trend at the studied period (Table 2 and Fig. 8).

Similar variability in monthly trends is identified for Passage B, although the SIAF trends are generally higher than those of A (Table 2). The increased SIM during the winter months occurs in concert with a decreased SIC (Figs 8a–e, i). The negative SIAF trends continuing from June to November are the combined effect associated with the decreasing trends in both the SIM and SIC fields (Figs 8f–k). For the south passage (C), the number of monthly SIAF trends that reach a significant value is relatively fewer (5 out of 12), and the negative SIAF trends persist for a longer period from June to December. Much larger declining SIC trends occur around this passage (Table 2). In FS, only two months (September and November) present significantly large positive SIAF trends (Table 2). The SIM and SIC trends are mostly

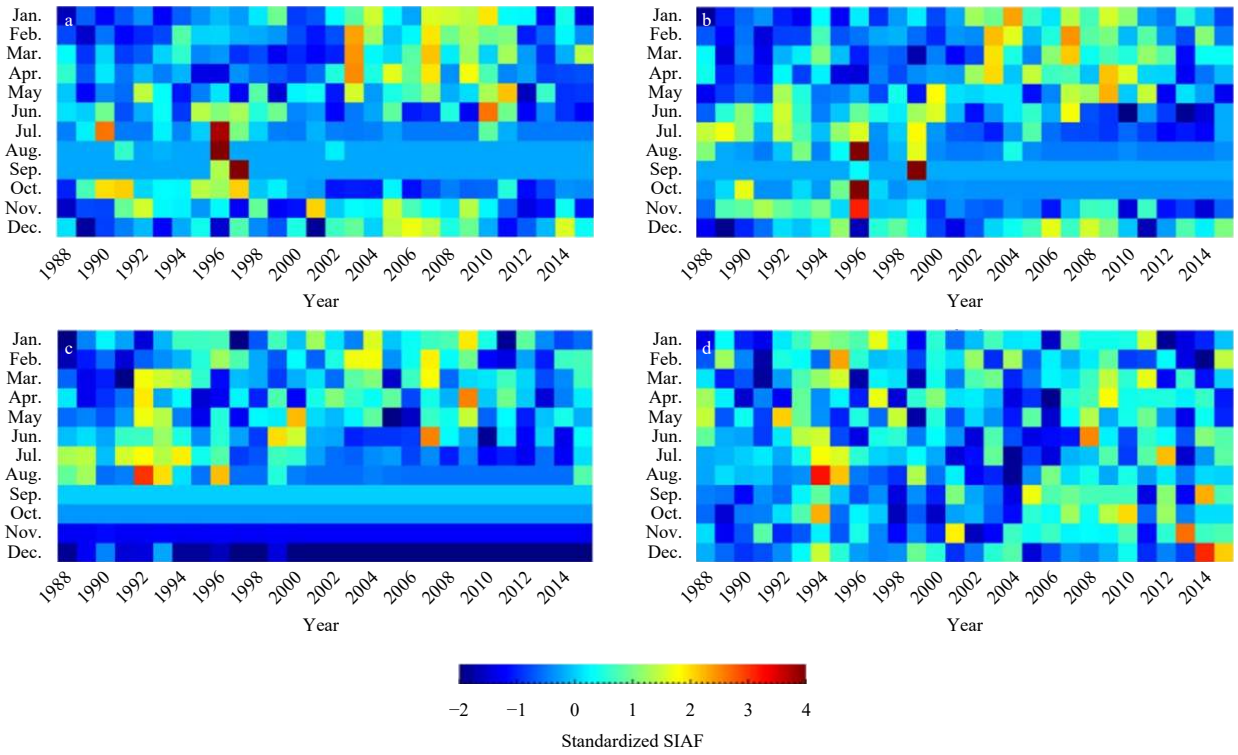

Fig. 7. Standardized monthly SIAF during 1988–2015.

Table 2. Trends in monthly and seasonal SIAF fields, and the corresponding trends in terms of SIM, SIC, and SLPG at the three passages of the Baffin Bay and FS over the period of 1988–2015

Passage		Jan.	Feb.	Mar.	Apr.	May	Jun.	Jul.	Aug.	Sep.	Oct.	Nov.	Dec.	Winter average (Oct.–May)	Summer average (Jun.–Sep.)
A	SIAF/ (10^3 km^2·(10 a)$^{-1}$)	15.07	14.01	12.56	5.16	2.86	−3.60	−1.41	−0.03	−0.17	−9.15	−0.05	13.80	6.78	−1.30
	SIM/(km·(10 a)$^{-1}$)	0.99	1.23	0.98	0.42	0.36	−0.29	−0.16	0.01	−0.02	−0.72	−0.14	1.08	0.53	−0.12
	SIC/(%·(10 a)$^{-1}$)	−0.75	−0.79	−0.56	−0.42	−5.78	−13.42	−6.72	−1.46	−1.29	−13.97	−2.85	−1.12	−3.28	−5.72
	SLPD/ (Pa·(10 a)$^{-1}$)	−0.10	0.31	0.00	0.29	0.26	−0.70	−0.62	−0.32	0.51	0.24	0.60	0.19	0.22	−0.28
B	SIAF/ (10^3 km^2·(10 a)$^{-1}$)	20.59	17.49	12.90	10.29	3.89	−5.83	−7.91	−0.95	−0.01	−3.48	−16.38	12.81	7.26	−3.68
	SIM/(km·(10 a)$^{-1}$)	1.25	1.30	0.85	0.71	0.31	−0.34	−0.72	−0.15	−0.002	−0.30	−1.12	0.93	0.49	−0.30
	SIC/(%·(10 a)$^{-1}$)	−2.63	−0.98	−0.29	−0.47	−3.06	−9.35	−13.07	−2.67	−0.13	−4.43	−11.69	−6.24	−3.72	−6.31
	SLPD/ (Pa·(10 a)$^{-1}$)	0.07	0.40	−0.17	0.30	0.04	−0.85	−0.40	−0.52	0.38	0.09	0.01	0.36	0.14	−0.35
C	SIAF/ (10^3 km^2·(10 a)$^{-1}$)	6.30	8.42	4.72	4.98	0.10	−2.49	−4.92	−0.73	0.00	−0.15	−10.32	−9.86	0.52	−2.04
	SIM/(km·(10 a)$^{-1}$)	0.48	0.75	0.47	0.43	0.05	−0.10	−0.44	−0.11	0.00	−0.02	−0.80	−0.57	0.10	−0.16
	SIC/(%·(10 a)$^{-1}$)	−9.67	−6.94	−4.56	−4.03	−5.74	−7.00	−9.68	−1.52	0.00	−0.43	−9.38	−9.37	−6.27	−4.55
	SLPD/ (Pa·(10 a)$^{-1}$)	−0.18	0.22	−0.62	0.62	0.00	−0.76	−0.38	−0.24	0.22	0.22	−0.28	−0.06	−0.01	−0.29
FS	SIAF/ (10^3 km^2·(10 a)$^{-1}$)	−2.60	−3.06	5.56	2.64	−3.10	0.42	−0.92	−1.63	7.46	8.18	11.96	6.89	3.31	1.33
	SIM/(km·(10 a)$^{-1}$)	−0.42	−0.26	0.43	0.17	−0.26	0.05	−0.04	−0.22	0.44	0.57	0.96	0.63	0.23	0.06
	SIC/(%·(10 a)$^{-1}$)	−0.93	−3.10	−1.96	0.13	−1.43	−0.58	−3.26	3.83	2.35	−2.27	−1.94	−3.69	−1.90	0.59
	SLPD/ (Pa·(10 a)$^{-1}$)	−0.90	0.15	0.88	0.38	0.11	1.00	0.95	1.22	0.50	0.51	1.03	0.10	0.28	0.92

Note: The confidence levels are marked with varying colors. Red, blue, and gold imply a significance at the 99%, 95%, and 90% levels, respectively.

insignificant and primarily cancelled out by each other. Therefore, the significant monthly SIAF trends are less common in the FS, which is consistent with the prior findings as provided by Kwok (2009).

The significant positive trends in monthly SIAF are observed in Passages A and B for the winter months (October–May) on the average order of 6.78×10^3 km^2/(10 a) and 7.26×10^3 km^2/(10 a), respectively (Table 3). In contrast, a slight positive trend occurs at C (0.52×10^3 km^2/(10 a)). For the summer months (June–September), the average declining SIAF trends over the Baffin Bay passages

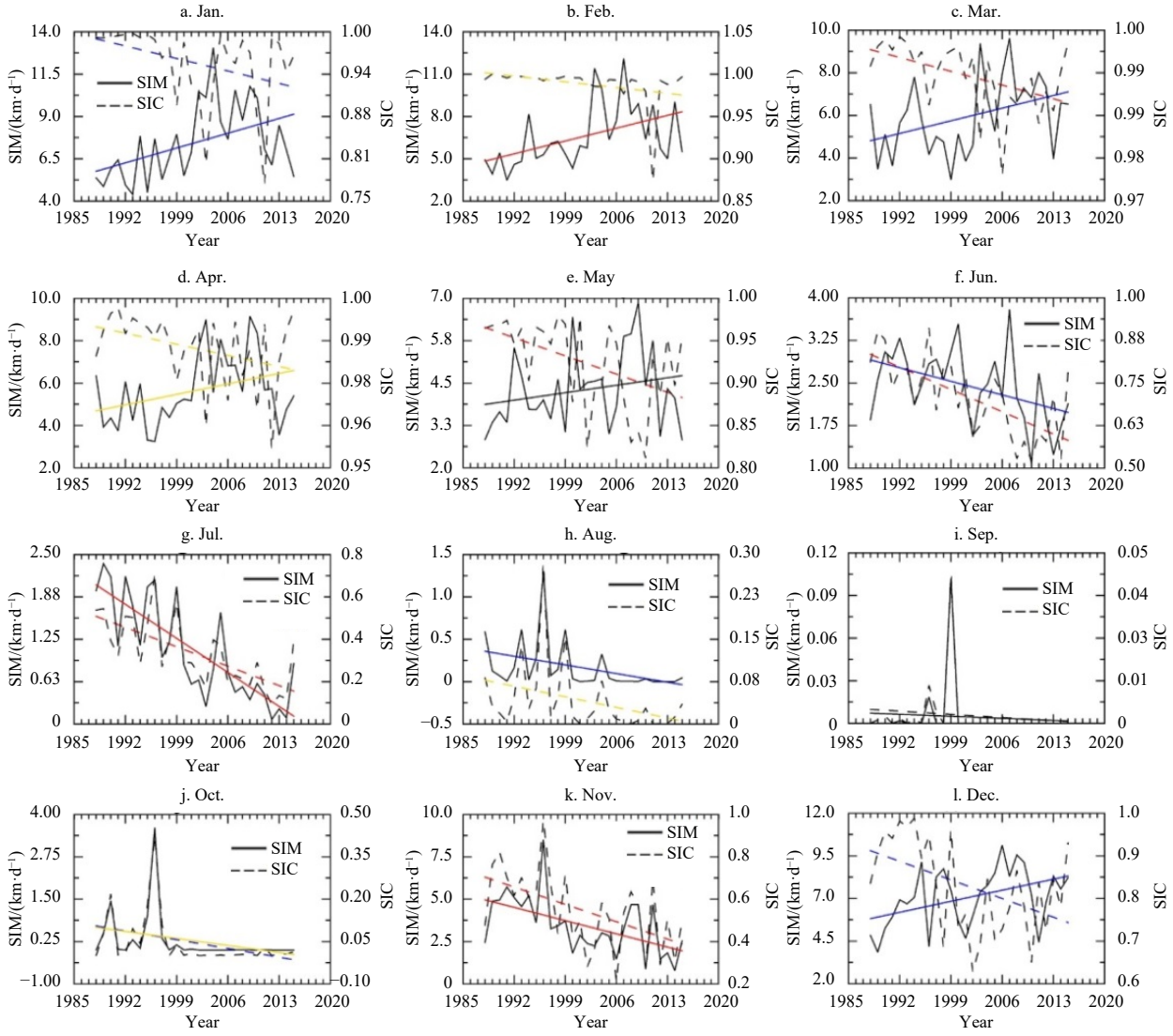

Fig. 8. Time series for the monthly mean SIM (bold line) and SIC (dash line) fields at Passage B. The trend line plot is added, with red, blue, and gold color denoting the significance levels at 99%, 95%, and 90%, respectively. The black line represents the trend that is not statistically significant.

Table 3. Mean annual and seasonal accumulated SIAF for different periods

Passage	SIAF/(10^3 km^2)		
	1988–2000	2000–2015	1988–2015
A	489/464/25	616/603/13	555/535/20
B	592/534/58	686/656/30	642/597/45
C	545/509/46	536/514/22	541/511/30
FS	692/610/82	720/624/96	707/616/91

Note: Numbers in the form of "N1/N2/N3" are referred as to the annual, winter, and summer SIAF fields, respectively. The winter and summer SIAF estimates cover for the periods of October–May and June–September, respectively.

reach to –1.30×10^3 km^2/(10 a) (A), –3.68×10^3 km^2/(10 a) (B), and –2.04×10^3 km^2/(10 a) (C), which is in contrast to the positive trend in FS (1.33 ×10^3 km^2/(10 a), Table 3).

3.3.3 *Variability and trends for seasonally and annually accumulated sea ice exports*

Figures 9 and 10 show the time series of the annual (October to the following September) accumulated SIAF and the respective SIM and SIC record over the period of 1988/1989 to 2014/2015. The mean annual SIAFs for the three of Baffin Bay passages over this period are 555×10^3 km^2 (A), 642×10^3 km^2 (B), and 541×10^3 km^2 (C). These amounts are less than that via the FS (707×10^3 km^2). A decadal increase of the annual SIAF is evident for the Passages A and B (Figs 10a and e) between the two periods of 1988–2000 and 2001–2015. For Passage A, the mean annual SIAFs increased by 127 km^2 for the period before and after 2000, from 489×10^3 km^2 to 616×10^3 km^2 (Table 3). For Passage B, the mean annual SIAFs increased by 94 ×10^3 km^2 for the period from 592×10^3 km^2 (before 2000) to 686×10^3 km^2 (after 2000). Indeed, such evident decadal changes lead to an overall increasing trend, as illustrated in the annual SIAF record for the two passages (Figs 10a and e). Specifically, Passages A and B present the significant trends of 53.1×10^3 km^2/(10 a) and 41.2×10^3 km^2/(10 a), respectively. In contrast, the annual SIAF trends at Passages C and FS reveal insignificant trends (Figs 10i and m), and the decadal changes are not prominent (Table 3).

For Passages A and B, the increasing SIAF trends (Figs 10b and f) are primarily caused by positive SIM trends. The negligible

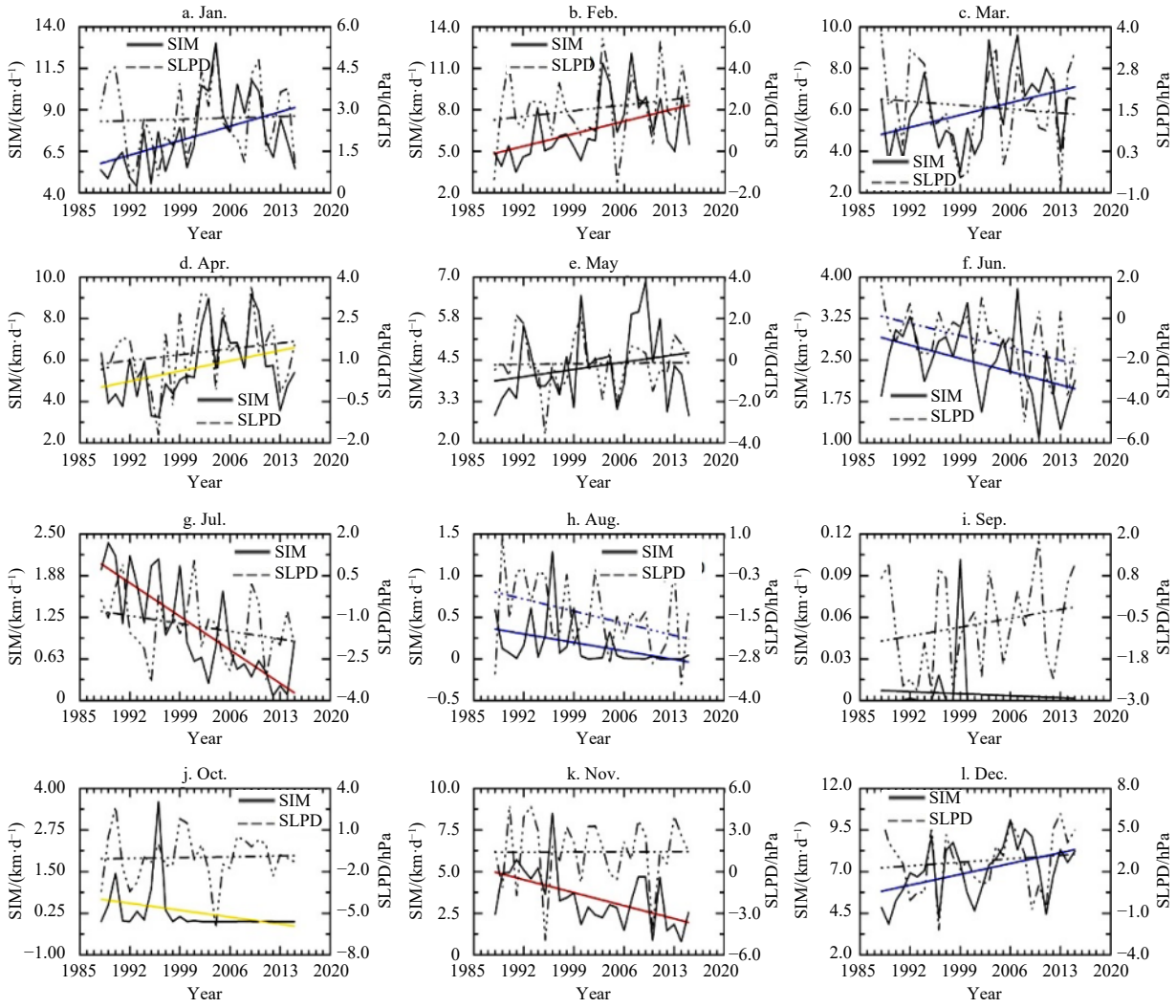

Fig. 9. Time series of the monthly mean SIM fields (bold line) together with cross-gate sea level pressure difference (SLPD, dash line) at Passage B. The linearly fitted trend is also shown. The red, blue, and gold color indicates a significance at the 99%, 95%, 90% levels, respectively. The black linear line represents the trend that is not statistically significant.

SLPD trends appear to play a minor role (Figs 10d and h). A slight negative SIAF trend is found in Passage C (Fig. 10i). Compared with the three passages in the Baffin Bay, the FS shows a relatively significant trend with regard to the annual mean SLPD on the order of 0.43 hPa/(10 a) significant at the 90% level (Fig. 10p). As a result, SLPD plays a vital role in the positive trends of SIM (0.16 km/(10 a)) and SIAF (29.4×10^3 km^2/(10 a)). With respect to the SIC fields, the declining trends for the three Baffin Bay passages (from –4.5%/(10 a) to –6.0%/(10 a)) are significant in relative to that of the FS (–1.0%/(10 a)).

The winter sea ice export primarily determines the variability and trends of the annual SIAF from October to next May. Concerning the three Baffin Bay passages, no less than 93% on average of the annual SIAF is attributable to winter export for the period of 1988/1989 to 2014/2015 (Fig. 11). By comparison, the winter export is comparatively lower for the FS (87%). Moreover, the average winter SIAF contribution to the annual SIAF was augmented by 2%–6% (Fig. 11) during the later period (2001–2015) in comparison with the earlier period (1988–2000). However, a decline of approximately 2% is noted for the wintertime contribution to the annual SIAF through FS (Fig. 11). Based on the annual ice export budget, the higher percentage of winter sea ice export suggests that the contribution from the summer export declines, and vice versa.

3.3.4 *Sea ice transport within the Baffin Bay*

The net sea-ice transport is an indicator of the ability to reserve sea ice for a defined regime, and it is estimated as the SIAF difference (SIAFD) between two adjacent passages. For instance, SIAFD_AB corresponds to the SIAF difference between those of via Passages A and B (i.e., SIAF_A – SIAF_B). A positive value suggests a net ice inflow (convergence), whereas a negative value refers to a net outflow (divergence). Table 4 lists the statistical results for the net sea ice transport between different passages in the Baffin Bay over the period of 1988/1989 to 2014/2015. Annually, a distinct net annual outflow (–87.3×10^3 km^2/a, on average) is identified in the northern Baffin Bay (the areas between Passages A and B, SIAFD_AB). For SIAFD_AC, the regime between Passages A and C, approaches to a nearly balanced state in terms of sea ice inflow and outflow, with a small amount of net input of 14.3×10^3 km^2/a (Table 4). In addition, a much larger mean value of annual SLPD_BC, on the order of 101.6×10^3 km^2/a, is suggest-

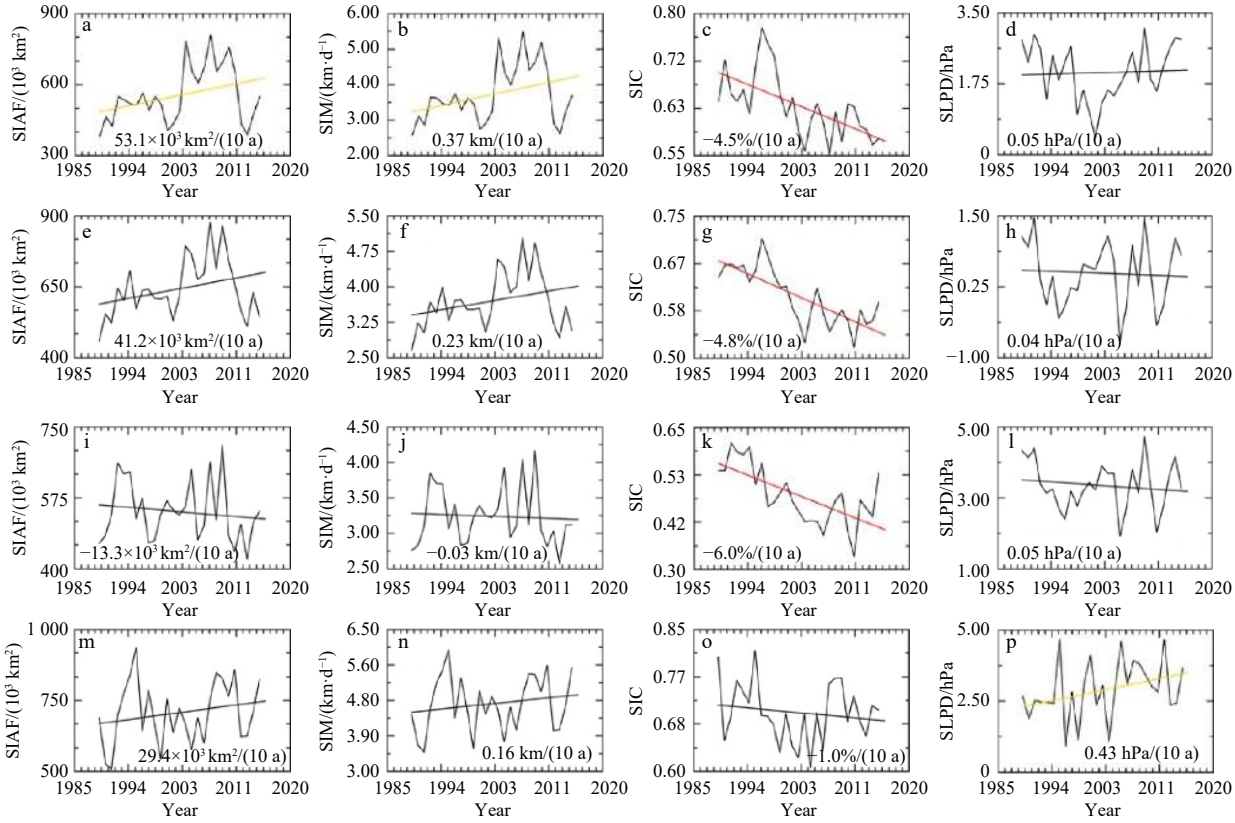

Fig. 10. Time series for the annual SIAF (October to following September) through different passages. The *x*-axis label denotes the year of September. For example, the year "1994" indicates the annual cycle from October to the following September in 1993/1994. The annual mean SIM, SIC, and SLPD fields are also given in the second, third, and fourth columns, respectively. The Linearly fitted trend is marked by the red, blue, and gold lines, corresponding to the significance levels at 99%, 95%, 90%, respectively.

ive of a sea ice reservoir in the southern Baffin Bay (i.e., the regime between Passages B and C).

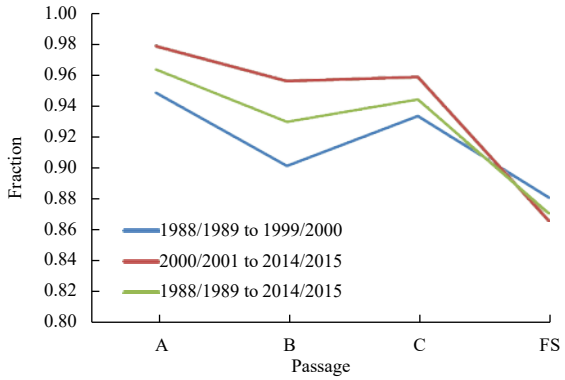

Fig. 11. The fraction of winter SIAF relative to the annual SIAF for different periods through varying passages.

Table 4. Statistical results for the net annual SIAF (1988/1989 to 2014/2015) between the different passages in the Baffin Bay

	SIAFD_AB	SIAFD_BC	SIAFD_AC
Mean/(10^3 km^2)	−87.3	101.6	14.3
Standard deviation/(10^3 km^2)	57.7	87.8	118.6
Trend/(10^3 km^2·(10 a)$^{-1}$)	11.9	64.2	54.5

Note: The red and blue color denote the trends that are significant at the levels of 99% and 95%, respectively.

Monthly variability for the net ice transport between different passages are shown in Fig. 12. For SIAFD_AB, negative values greater than −25×10^3 km^2 (i.e., net sea ice outflow) occur for most months, except for January and February (Fig. 12, black line) when a net positive sea ice inflow of less than 40×10^3 km^2 is observed. For SIAFD_AC, positive quantities smaller than 70×10^3 km^2 (net sea ice inflow) are found for the period from January to March, whereas negative values (i.e., net outflows) not ex-

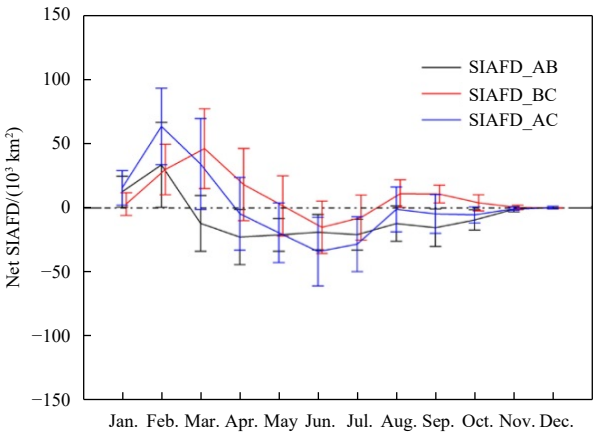

Fig. 12. Mean net monthly SIAFD between different passages in the Baffin Bay over the period of 1988/1989 to 2014/2015. The Error bar corresponds to the standard deviation.

ceeding –35×10³ km² emerge for the remaining months (Fig. 12, blue line). Regarding the SIAFD_BC, larger positive amounts (lower than 50×10³ km²/month) are found over the later winter period from February to April, whereas smaller positive values (below 10×10³ km²/month) are encountered for the period of August to November (Fig. 12, red line). The negative values in SIAFD_BC greater than –15×10³ km²/month occur during the midsummer months (June to July). As a reservoir pool of sea ice (as mentioned above), the net positive sea ice transport between Passages B and C (SIAFD_BC) is primarily dictated by those during February to April (on average, up to 40×10³ km²/month as shown in Fig. 12 which is marked by the red line).

We further analyze the trend in the net annual SIAF (Fig. 13). SIAFD_AB presents a clear trend (11.9×10³ km²/(10 a)), whereas the other two reveal significant positive trends of 54.5×10³ km²/(10 a) (SIAFD_AC) and 64.2×10³ km²/(10 a) (SIAFD_BC). This again suggests that the Baffin Bay, especially the southern part between Passages B and C, tends to present more converged sea ice over time. With respect to SIAFD_AC and SIAFD_BC, the increasing trends are mainly associated with the larger winter net ice export from December to May (Table 5). Notably, the highest net ice flux of 23×10³ km²/(10 a) occurs in December (Table 5), which is related to the increasing SIAF trend in A and B of up to 13×10³ km²/(10 a) together with a decreasing SIAF trend in C of approximately –9×10³ km²/(10 a) (Table 2). Seasonally, the accelerated trends for ice inflow through A or B during the winter and spring months (from January to May) are consistent with the relatively slower sea ice outflow via C (Table 2). During the summer months (June–August), a positive SLPD_AB trend accompanies a negative trend in SLPD_BC. As summarized in Table 2, these trends are mainly caused by a faster decline of the SIAF through the Passage B during the summer months (–3.68×10³ km²/(10 a)), compared with the negative trends in the other two passages (–1.30×10³ km²/(10 a) for A and –2.04×10³ km²/(10 a) for B).

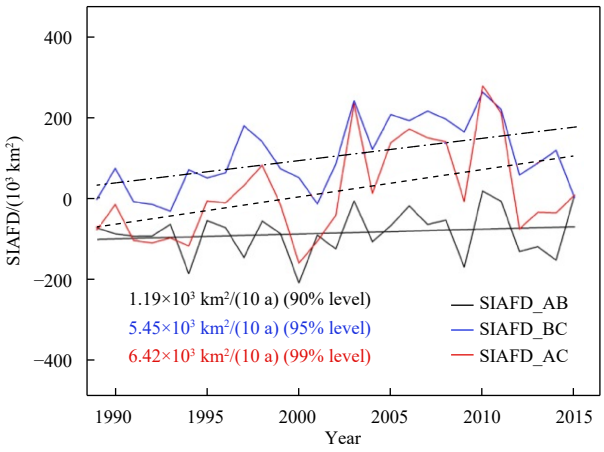

Fig. 13. Net annual SIAFD between the different Baffin Bay passages. For example, SIAFD_AB is the difference between SIAF through the Passages A and B. Linear trend is added, with the bold, dash, and dash-dot lines representing the trends that are significant at the 90%, 95%, and 99% levels, respectively.

Table 5. Trends for the monthly SIAF difference through the different Baffin Bay passages

	Jan.	Feb.	Mar.	Apr.	May	Jun.	Jul.	Aug.	Sep.	Oct.	Nov.	Dec.
SIAFD_AB/(10³ km²·(10 a)⁻¹)	–5.51	–3.47	–0.34	–5.12	–1.03	2.23	6.49	0.92	–0.16	–5.67	16.43	0.99
SIAFD_BC/(10³ km²·(10 a)⁻¹)	14.29	9.06	8.18	5.31	3.79	–3.34	–2.98	–0.22	0.01	–3.33	–6.06	22.66
SIAFD_AC/(10³ km²·(10 a)⁻¹)	8.78	5.59	7.84	0.19	2.76	–1.12	3.51	0.70	–0.17	–9.00	10.36	23.66

Note: Red, blue, and gold color denotes the trends that are significant at the levels of 99%, 95%, and 90%, respectively.

4 Discussion

4.1 *Linkages to changes in climate factors*

The abrupt decadal changes in the annual (Figs 10a and e) and winter SIAF fields (Table 2) are apparent for the north and middle passages of the Baffin Bay. In this section, we investigate four climatic factors, including the surface wind (SW), sea level pressure (SLP), SAT, and SST, which may contribute to these changes. All of the used climatic variables are obtained from the NOAA NECP/NCAR reanalysis products (Kalnay et al., 1996).

The differences of the local SW between two periods, defined as P1 (1988–2000) and P2 (2001–2015), vary with season (Figs 14a and b). For the winter period (October–May), the inter-period differences (P2–P1) show that the southeastward SW fields, with magnitudes mostly less than 0.4 m/s, dominate over Passages A and B (Fig. 14a), which is consistent with the increasing trend in the SIAF as observed during winter (Table 2). In addition, the anomalous easterly SW (0.3–0.4 m/s) to the south of Davis Strait would push sea ice against the Baffin Island in the west (Fig. 14a); hence, it may have exerted influences on boosting a southward sea ice advection through the southern Passage C. As a result, the average trend of the wintertime monthly SIAF between P1 and P2 (roughly 0.51×10³ km²/(10 a), as shown in Table 3), and the decadal change of winter (October–May) sea ice export by approximately 5×10³ km² (Table 4), from 509×10³ km² (P1) to 514×10³ km² (P2), are not readily evident for Passage C. During the summer seasons (Fig. 14b), the inter-period changes of the SW fields in the Baffin Bay mainly present a northwestward direction, with increasing magnitudes from southern to northern Baffin Bay (as indicated by background color in Fig. 14b). To be specific, the average declining trend in the SW magnitude is as follows: –1.1 m/s for Passage A, –0.8 m/s for Passage B, and –0.6 m/s for Passage C (Fig. 14b). This decline is associated with the negative summer SIAF trend as observed for each passage in the Baffin Bay (Table 2, June–August).

The spatial layout in the SLP, on the other hand, sheds light on the role of the geostrophic winds in the modulation of the sea ice transport through the Baffin Bay (Figs 14c and d). For the winter period, the inter-period SLP changes, with higher SLPs (on average, approximately 0.9 hPa) in the western Baffin Island and relatively lower SLPs (approximately 0.6 hPa) in the Baffin Bay (Fig. 14c), seem to support a northwesterly wind movement through Passages A and B. Lower SLPs (approximately 0.4 hPa) are observed in the area close to the southern passage (C) as well as in northern Labrador Sea (Fig. 14c). This SLP distribution pattern has the potential to promote a westward air movement, which is broadly consistent with the local surface winds as shown in Fig. 14b. In summer, the higher SLPs (approximately 2.5 hPa) over the east side of Baffin Bay (Greenland coasts) along with the lower SLP (about 0.5 hPa) over the west side (Fig. 14d) are favorable for a northwestward movement for the air mass around the Baffin Bay area (Fig. 14b). Broadly, the changes of SLP

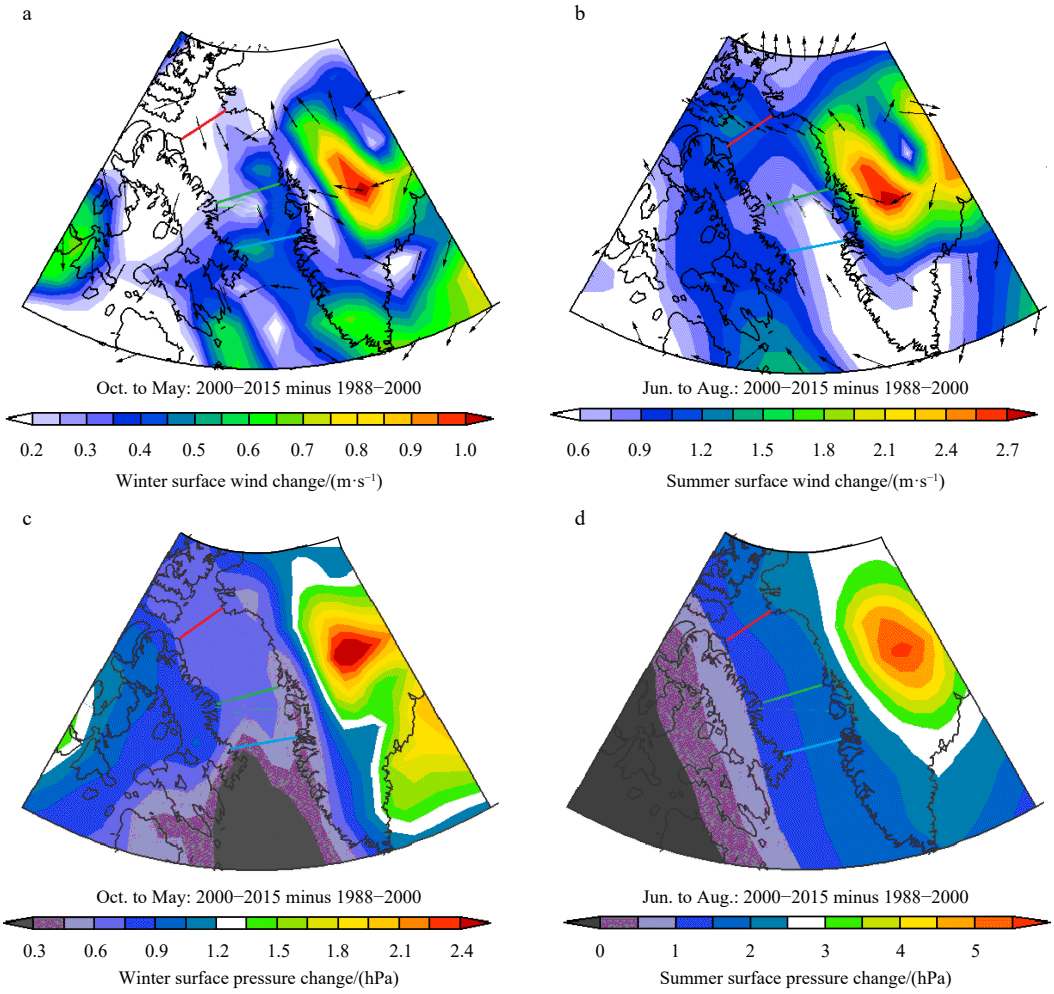

Fig. 14. Inter-period changes (P2–P1) of surface wind (SW) for the winter (October–May, a) and summer (June–August, b) between P1 (1988–2000) and P2 (2001–2015), and the corresponding sea level pressure (SLP) changes for the winter (c), and summer (d). The red, green, and blue lines in the Baffin Bay correspond to Passages A, B, and C, respectively.

distribution are consistent with the spatial variations of SW, which is largely in phase with the spatiotemporal changes of sea ice export through different passages over the Baffin Bay.

Furthermore, we examined the changes of two climatic factors (SAT and SST) to interpret the Baffin Bay sea ice export variations in the context of an amplified warming climate in the Arctic (Serreze et al., 2009; Screen et al., 2012). Between the two periods (P2–P1), the SAT and SST are reinforced for certain seasons (Fig. 15). The warmer surface air and upper ocean are consistent with facts reported by Zweng and Münchow (2006), and generally congruent with the notable reduction in SIC fields, as highlighted in Fig. 10 and Table 2.

During the winter months, the declining trend in the SIC over different passages is significant (Table 2) and consistent with the warmer SAT (Fig. 15a) and SST fields (Fig. 14b) throughout the bay. Notably, the warmest winter SAT (mostly above 3.5 K, Fig. 15a) and SST (dominantly beyond 4.0 K, Fig. 15c) appear in the southeastern part of Baffin Bay, covering the major portion of Passage C. Accordingly, a larger winter SIC reduction (–6.27%/(10 a)) is observed especially over this passage. The enhanced SAT and SST may also play a vital role in the significant decline in SIC at Passages A (–3.27%/(10 a)) and B (–3.72%/(10 a)).

Over the summer period, the temporal variations of the SAT and SST are more prominent over the central part of Baffin Bay (Figs 15b and d), which is consistent with the most significant decline of the SIC at Passage B (–6.31%/(10 a)) during summer (Table 2). The SAT and SST increases are relatively weak in Passage A (0.8 K and 0.6 K, on average) compared to those of Passage C (0.9 K and 1.1 K). However, a slightly larger declining in SIC is found at the Passage A (–5.72%/(10 a)) than that in Passage C (–4.55%/(10 a)). This can be explained by the continued occurrence of a large polynya (the North Water Polynya) in the north of the bay which allows for the exposure of abundant open water to trigger the positive ice-albedo feedback (Melling et al., 2001). More dark water will absorb greater amounts of solar energy, which can melt more sea ice, such that a swifter summer reduction in SIC is expected at Passage A than Passage C. Overall, the remarkable SIC declines, along with the winds blowing northwestward (Fig. 14b), appear to impose combined influences on the summer negative SIAF trends for the passages in the Baffin Bay, which are –1.3×10^3 km^2/(10 a), –3.68×10^3 km^2/(10 a), –2.04×10^3 km^2/(10 a) at Passages, A, B, and C, respectively (Table 2).

4.2 *Connections to the atmospheric variability*

The NAO represents the dominant mode of atmospheric variability over the northern North Atlantic Ocean, and it is closely

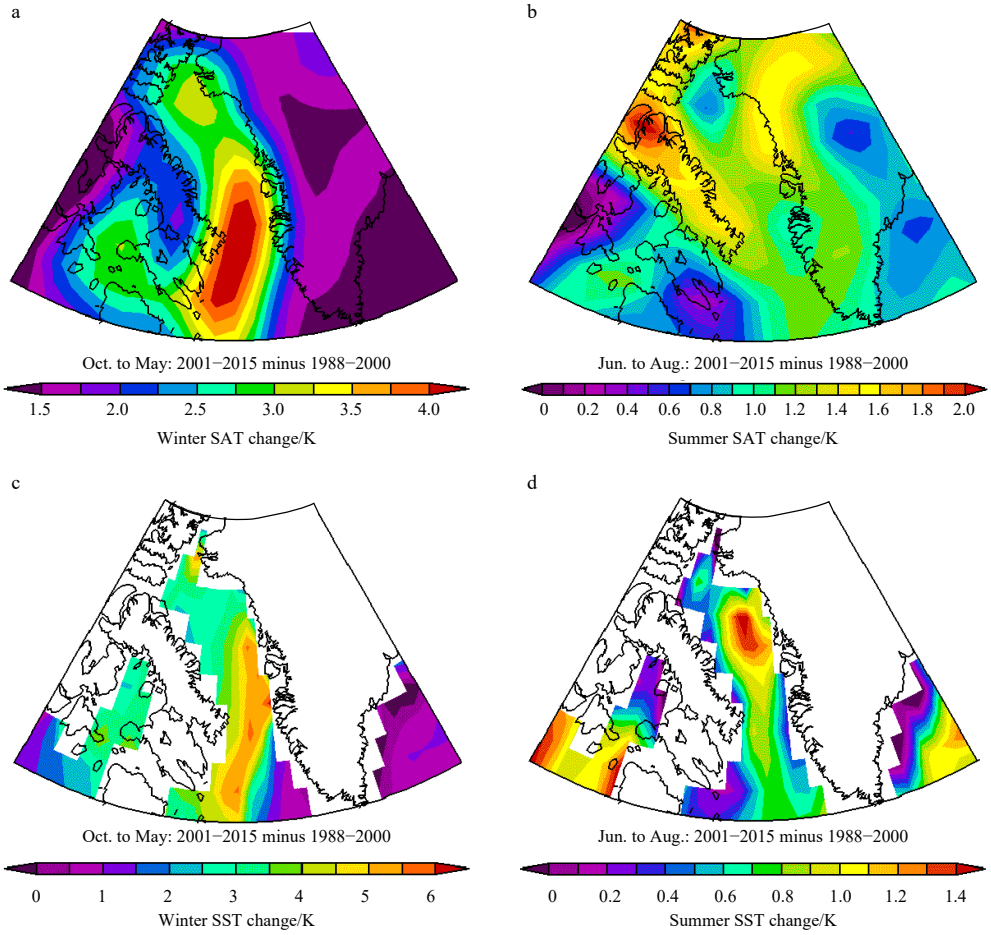

Fig. 15. Inter-period changes (P2–P1) of surface air temperature (SAT) between P1 (1988–2000) and P2 (2001–2015) for the winter (October–May, a) and summer (June–August, b), and the sea surface temperature (SST) changes for the winter (c) and summer (d) seasons.

related to the midlatitude Azores high and the sub-polar Icelandic low-pressure systems. In the positive/negative NAO phase, the SLP is deeper/shallower over the Icelandic low, the atmospheric circulation becomes stronger/weaker, and northerly/southerly wind likely flows through the Baffin Bay (Häkkinen and Cavalieri, 2005) and the FS (Kwok, 2000, 2009; Kwok et al., 2004). These changes could in part account for the variability of the sea ice extent in the Baffin Bay and Labrador Sea (Kvamstø et al., 2004). However, Fig. 16 suggests that the monthly SIAF is only slightly correlated with the NAO index for the three passages through the Baffin Bay (R=0.23–0.32). Furthermore, only a weak connection occurs between the monthly SIAF through the FS and NAO over the period of 1988–2015 (R=0.15). However, this does not indicate that NAO plays a minor role in modulating the interannual variability of sea ice drift and export in the Arctic Ocean outlets (Kwok et al., 2013). Previous studies have reported a robust temporal sensitivity of the FS sea ice export to the NAO index for the periods of 1979–1996 (R=0.66) and 1979–2007 (R=0.60) (Kwok, 2009). This temporal sensitivity in association with the NAO also occurs in the Baffin Bay passages for the two periods (1988–1996, 1988–2015): A (R=0.41, 0.22), B (R=0.45, 0.24), and C (R=0.49, 0.30).

The SLPD across a passage represents the local atmospheric forcing and is closely related to the monthly SIAFs through the Baffin Bay passages (Fig. 17). The correlation at the Baffin Bay (R: 0.69–0.71) is marginally weaker than that for the FS (R=0.74). The Baffin Bay is confined by land in the west (Baffin Island) and east (Greenland). Therefore, the sea ice drift pattern in the Baffin Bay may be readily subject to the orographic configuration. In contrast, the dynamic effect of sea ice over the FS area is relatively less susceptible to the Svalbard Island to the east (Kwok et al., 2004). This implies a slightly higher degree of free sea ice drift, and thus a relatively stronger connection of ice export with the local atmospheric circulation in FS.

5 Conclusions

The satellite-derived sea ice area exported through the three passages in the Baffin Bay was obtained over the period 1988–2015. The comparisons show that our SIAF estimates are consistent with the previous results. For the Baffin Bay passages, the trends and changes in the SIAF fields are spatiotemporally varying. Seasonally, the increasing (decreasing) trends in SIAF is observed during the winter (summer) months. Regionally, an increasing trend of the annual SIAF is identified for the north and middle passages (referred to as A and B), whereas an insignificant negative trend is found in the south passage (referred to as C). The obvious positive trend in the SIAF through A and B, together with a slight negative trend through C, combined to produce

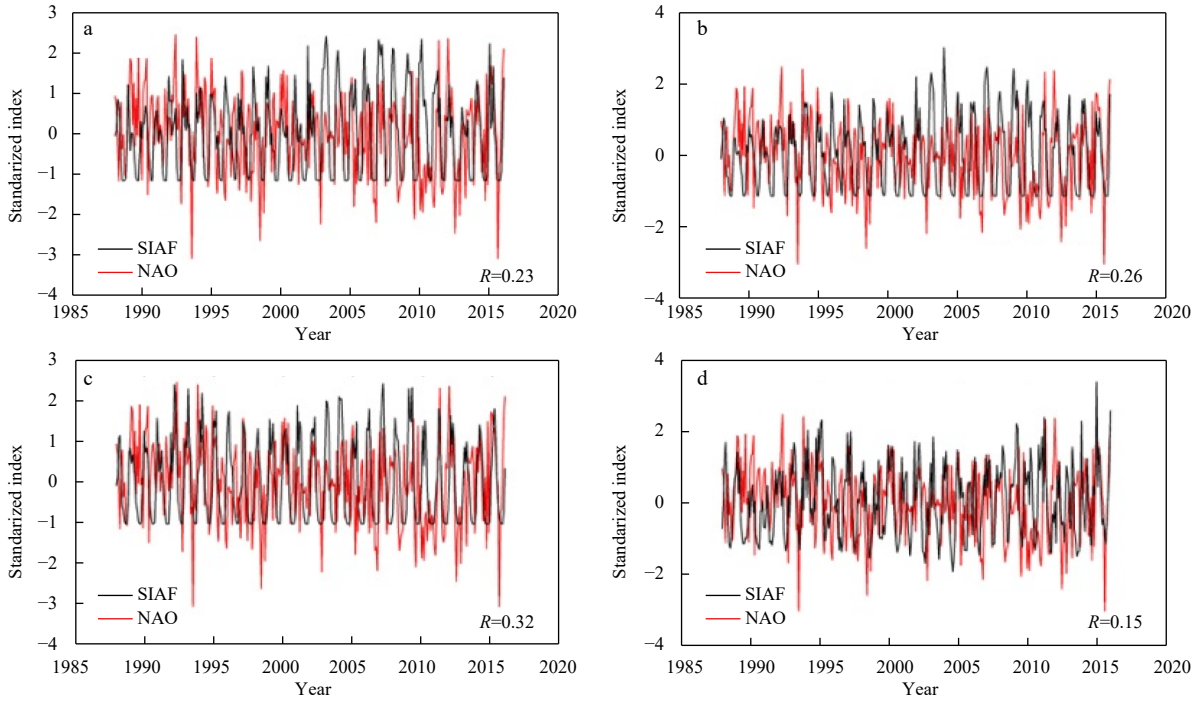

Fig. 16. Time series of the monthly SIAF through the Baffin Bay Passages A (a), B (b), and C (c), and FS (d), together with the corresponding monthly mean NAO index. To facilitate our analysis, the two variables have been standardized. In short, the monthly SIAF values (or monthly-mean NAO values) are first subtracted from the corresponding mean monthly value over the period 1988–2015 and then divided by the standard deviation of the values considered.

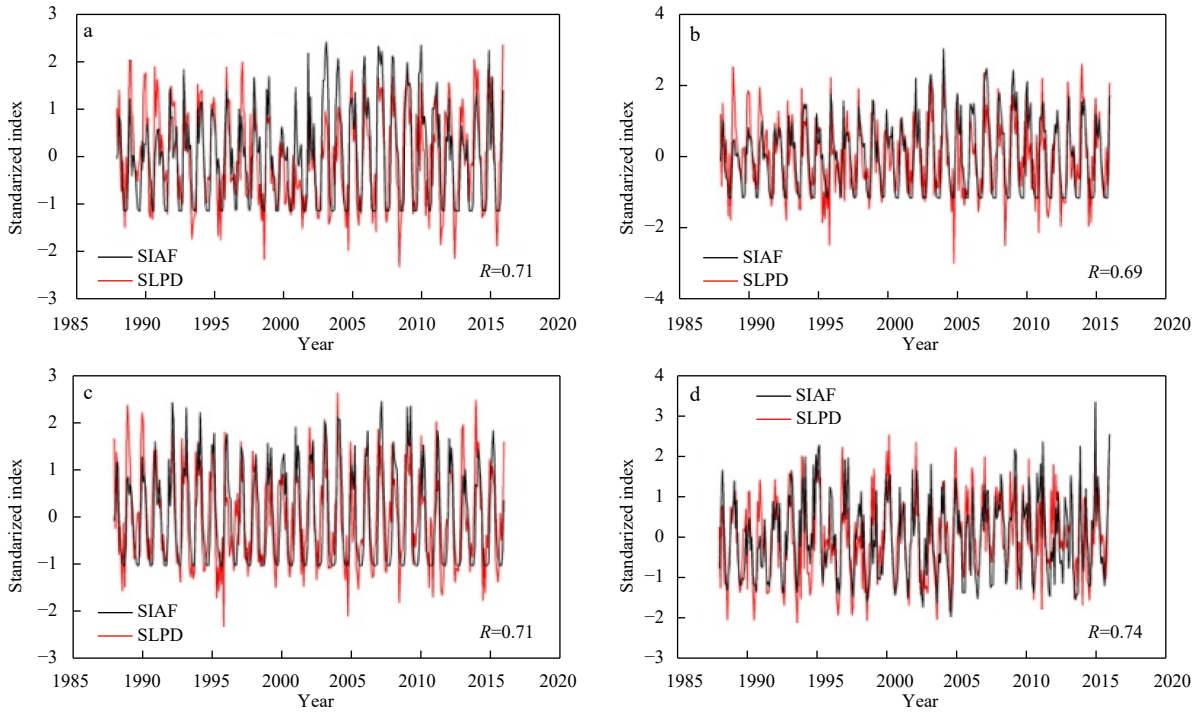

Fig. 17. Time series of the monthly SIAF via the different Baffin Bay Passages (including A (a), B (b), and C (c)), and those via FS (d), as well as the monthly mean SLPD fields. The fields are standardized, as depicted in Fig. 16.

a pattern of sea ice convergence in the southern Baffin Bay.

The changes and variability in SIAF over the Baffin Bay passages are primarily determined by the SIM variations associated with the variability in SW, SLP, SIC fields. The SIC fields exhibit a significant decline at all months that is in part linked to the warmer SAT and SST. The reduced SIC may also have contribute to the increasing trend in SIM, as observed for Passages A and B (Fig. 10). Compared with FS (Kwok, 2009), the cross-gate SLPD

for all the passages of Baffin Bay does not present a significant trend and thus accounts for very few to the the trend in SIAF. Indeed, the trends of Baffin Bay sea ice outflow is mainly attributable to the increased surface drag coefficient and decreased sea ice thickness (Bi et al., 2019).

A decadal increase of the annual SIAF is identified over Passages A and B between the two periods: 1988–2000 and 2001–2015. Before and after 2000, Passage A is observed with an increase in the annual SIAF by 127 km^2, approximately from 489×10^3 km^2 to 616×10^3 km^2. The mean annual SIAF in Passage B increases by 94 ×10^3 km^2 for the same periods from 592×10^3 km^2 to 686×10^3 km^2, respectively. The annual SIAFs via Passages A and B present a significant trend of 53.1×10^3 km^2/(10 a) and 41.2×10^3 km^2/(10 a), respectively. In contrast, the annual SIAF trends in Passages C and FS show insignificant trends, and the corresponding decadal changes are not clear.

Over the investigated period (1988–2015), the monthly sea ice export through the Baffin Bay passages is overall weakly connected to the atmospheric circulation pattern related to NAO. Similar to sea ice outflow through the FS (Kwok, 2000; Kwok et al., 2004, 2013), the association with the NAO is sensitive to the period examined. In addition, a relatively robust connection is observed between the monthly sea ice export and the SLPD (R is about 0.70 for the Baffin Bay passages). Considering that the Baffin Bay is constrained mainly by land in the west (Baffin Island) and east sides (Greenland), it is unsurprising the sea ice drift in the Baffin Bay may not be as free as that in the FS (R=0.74).

Acknowledgement

We thank the data providers as follows. NSIDC provides the satellite-derived ice motion and concentration data; National Centers for Environmental Prediction/National Center for Atmospheric Research (NCEP/NCAR) provides the reanalysis product.

References

Bi Haibo, Huang Haijun, Fu Min, et al. 2016a. Estimating sea-ice volume flux out of the Laptev Sea using multiple satellite observations. Polar Research, 35(1): 24875, doi: 10.3402/polar.v35.24875

Bi Haibo, Sun Ke, Zhou Xuan, et al. 2016b. Arctic sea ice area export through the fram strait estimated from satellite-based data: 1988–2012. IEEE Journal of Selected Topics in Applied Earth Observations and Remote Sensing, 9(7): 3144–3157, doi: 10.1109/JSTARS.2016.2584539

Bi Haibo, Zhang Zehua, Wang Yunhe, et al. 2019. Baffin Bay sea ice inflow and outflow: 1978–1979 to 2016–2017. The Cryosphere, 13(3): 1025–1042, doi: 10.5194/tc-13-1025-2019

Cho K, Sasaki N, Shimoda H, et al. 1996. Evaluation and improvement of SSM/I sea ice concentration algorithms for the Sea of Okhotsk. Journal of the Remote Sensing Society of Japan, 16(2): 47–58

Comiso J C, Gersten R A, Stock L V, et al. 2017a. Positive trend in the Antarctic sea ice cover and associated changes in surface temperature. Journal of Climate, 30(6): 2251–2267, doi: 10.1175/JCLI-D-16-0408.1

Comiso J C, Hall D K. 2014. Climate trends in the Arctic as observed from space. Wiley Interdisciplinary Reviews: Climate Change, 5(3): 389–409, doi: 10.1002/wcc.277

Comiso J C, Meier W N, Gersten R. 2017b. Variability and trends in the Arctic Sea ice cover: Results from different techniques. Journal of Geophysical Research, 122(8): 6883–6900

Cuny J, Rhines P B, Kwok R. 2005. Davis Strait volume, freshwater and heat fluxes. Deep Sea Research Part I: Oceanographic Research Papers, 52(3): 519–542, doi: 10.1016/j.dsr.2004.10.006

Curry B, Lee C M, Petrie B, et al. 2014. Multiyear volume, liquid freshwater, and sea ice transports through Davis Strait, 2004–10. Journal of Physical Oceanography, 44(4): 1244–1266, doi: 10.1175/JPO-D-13-0177.1

Drinkwater K. 2009. Comparison of the response of Atlantic cod (*Gadus morhua*) in the high-latitude regions of the North Atlantic during the warm periods of the 1920s–1960s and the 1990s–2000s. Deep Sea Research Part II: Topical Studies in Oceanography, 56(21–22): 2087–2096

Goosse H, Fichefet T, Campin J M. 1997. The effects of the water flow through the Canadian Archipelago in a global ice-ocean model. Geophysical Research Letters, 24(12): 1507–1510, doi: 10.1029/97GL01352

Graham R M, Cohen L, Petty A A, et al. 2017. Increasing frequency and duration of Arctic winter warming events. Geophysical Research Letters, 44(13): 6974–6983, doi: 10.1002/2017GL073395

Häkkinen S, Cavalieri D J. 2005. Sea ice drift and its relationship to altimetry-derived ocean currents in the Labrador Sea. Geophysical Research Letters, 32(11): L11609, doi: 10.1029/2005GL022682

Hansen A S, Nielsen T G, Levinsen H, et al. 2003. Impact of changing ice cover on pelagic productivity and food web structure in Disko Bay, West Greenland: A dynamic model approach. Deep Sea Research Part I: Oceanographic Research Papers, 50(1): 171–187, doi: 10.1016/S0967-0637(02)00133-4

Hurrell J W. 1995. Decadal trends in the north atlantic oscillation: regional temperatures and precipitation. Science, 269(5224): 676–679, doi: 10.1126/science.269.5224.676

Kalnay E, Kanamitsu M, Kistler R, et al. 1996. The NCEP/NCAR 40-year reanalysis project. Bulletin of the American Meteorological Society, 77(3): 437–472, doi: 10.1175/1520-0477(1996)077<0437:TNYRP>2.0.CO;2

Krumpen T, Gerdes R, Haas C, et al. 2016. Recent summer sea ice thickness surveys in Fram Strait and associated ice volume fluxes. The Cryosphere, 10(2): 523–534, doi: 10.5194/tc-10-523-2016

Krumpen T, Janout M, Hodges K I, et al. 2013. Variability and trends in Laptev Sea ice outflow between 1992–2011. The Cryosphere, 7(1): 349–363, doi: 10.5194/tc-7-349-2013

Kvamstø N G, Skeie P, Stephenson D B. 2004. Impact of Labrador sea-ice extent on the North Atlantic oscillation. International Journal of Climatology, 24(5): 603–612, doi: 10.1002/joc.1015

Kwok R. 2000. Recent changes in Arctic Ocean sea ice motion associated with the North Atlantic Oscillation. Geophysical Research Letters, 27(6): 775–778, doi: 10.1029/1999GL002382

Kwok R. 2007. Baffin Bay ice drift and export: 2002–2007. Geophysical Research Letters, 34(19): L19501, doi: 10.1029/2007GL031204

Kwok R. 2009. Outflow of Arctic ocean sea ice into the Greenland and Barents Seas: 1979–2007. Journal of Climate, 22(9): 2438–2457, doi: 10.1175/2008JCLI2819.1

Kwok R, Cunningham G F, Pang S S. 2004. Fram Strait sea ice outflow. Journal of Geophysical Research: Oceans, 109(C1): C01009, doi: 10.1029/2003JC001785

Kwok R, Maslowski W, Laxon S W. 2005. On large outflows of Arctic sea ice into the Barents Sea. Geophysical Research Letters, 32(22): L22503

Kwok R, Pedersen L T, Gudmandsen P, et al. 2010. Large sea ice outflow into the Nares Strait in 2007. Geophysical Research Letters, 37(3): L03502

Kwok R, Spreen G, Pang S. 2013. Arctic sea ice circulation and drift speed: Decadal trends and ocean currents. Journal of Geophysical Research: Oceans, 118(5): 2408–2425, doi: 10.1002/jgrc.20191

Melling H, Gratton Y, Ingram G. 2001. Ocean circulation within the North Water polynya of Baffin Bay. Atmosphere-Ocean, 39(3): 301–325, doi: 10.1080/07055900.2001.9649683

Parkinson C L. 2014. Global sea ice coverage from satellite data: Annual cycle and 35-Yr trends. Journal of Climate, 27(24): 9377–9382, doi: 10.1175/JCLI-D-14-00605.1

Parkinson C L, Cavalieri D J. 2002. A 21 year record of Arctic sea-ice extents and their regional, seasonal and monthly variability and trends. Annals of Glaciology, 34(1): 441–446

Peterson I K, Pettipas R. 2013. Trends in air temperature and sea ice in the Atlantic Large Aquatic Basin and adjoining areas. Canadian Technical Report of Hydrography and Ocean Sciences, Dartmouth: Fisheries and Oceans Canada, 290.

Screen J A, Deser C, Simmonds I. 2012. Local and remote controls on observed Arctic warming. Geophysical Research Letters, 39(10): L10709

Serreze M C, Barrett A P, Stroeve J C, et al. 2009. The emergence of surface-based Arctic amplification. The Cryosphere, 3(1): 11–19, doi: 10.5194/tc-3-11-2009

Smedsrud L H, Halvorsen M H, Stroeve J C, et al. 2017. Fram Strait sea ice export variability and September Arctic sea ice extent over the last 80 years. The Cryosphere, 11(1): 65–79, doi: 10.5194/tc-11-65-2017

Smedsrud L H, Sirevaag A, Kloster K, et al. 2011. Recent wind driven high sea ice area export in the Fram Strait contributes to Arctic sea ice decline. The Cryosphere, 5(4): 821–829, doi: 10.5194/tc-5-821-2011

Spreen G, Kern S, Stammer D, et al. 2006. Satellite-based estimates of sea-ice volume flux through Fram Strait. Annals of Glaciology, 44(1): 321–328

Stern H L, Heide-Jørgensen M P. 2003. Trends and variability of sea ice in Baffin Bay and Davis Strait, 1953–2001. Polar Research, 22(1): 11–18

Stroeve J C, Markus T, Boisvert L, et al. 2014. Changes in Arctic melt season and implications for sea ice loss. Geophysical Research Letters, 41(4): 1216–1225, doi: 10.1002/2013GL058951

Stroeve J C, Schroder D, Tsamados M, et al. 2018. Warm winter, thin ice?. The Cryosphere, 12(5): 1791–1809, doi: 10.5194/tc-12-1791-2018

Sumata H, Lavergne T, Girard-Ardhuin F, et al. 2014. An intercomparison of Arctic ice drift products to deduce uncertainty estimates. Journal of Geophysical Research: Oceans, 119(8): 4887–4921, doi: 10.1002/2013JC009724

Tilling R L, Ridout A, Shepherd A. 2016. Near-real-time Arctic sea ice thickness and volume from CryoSat-2. The Cryosphere, 10(5): 2003–2012, doi: 10.5194/tc-10-2003-2016

Tschudi M, Meier W N, Stewart J S, et al. 2019. Polar Pathfinder Daily 25 km EASE-Grid Sea Ice Motion Vectors, Version 4. NASA, Boulder, Colorado, doi: 10.5067/INAWUWO7QH7B.

Wu Bingyi, Zhang Renhe, D'Arrigo R, et al. 2013. On the relationship between winter sea ice and summer atmospheric circulation over eurasia. Journal of Climate, 26(15): 5523–5536, doi: 10.1175/JCLI-D-12-00524.1

Yang Qian, Dixon T H, Myers P G, et al. 2016. Recent increases in Arctic freshwater flux affects Labrador Sea convection and Atlantic overturning circulation. Nature Communications, 7: 10525, doi: 10.1038/ncomms10525

Zhang Zehua, Bi Haibo, Sun Ke, et al. 2017. Arctic sea ice volume export through the Fram Strait from combined satellite and model data: 1979–2012. Acta Oceanologica Sinica, 36(1): 44–55, doi: 10.1007/s13131-017-0992-4

Zhang Xiangdong, Sorteberg A, Zhang Jing, et al. 2008. Recent radical shifts of atmospheric circulations and rapid changes in Arctic climate system. Geophysical Research Letters, 35(22): L22701, doi: 10.1029/2008GL035607

Zweng M M, Münchow A. 2006. Warming and freshening of Baffin Bay, 1916–2003. Journal of Geophysical Research: Oceans, 111(C7): C07016, doi: 10.1029/2005JC003093